Met. Mater. Int., Vol. 24, No. 1 (2018), pp. 195~204
doi: 10.1007/s12540-017-7324-2

Effect of Grain Size Inhomogeneity of Ingot on Dynamic Softening Behavior and Processing Map of Al-8Zn-2Mg-2Cu alloy

Di Feng[1,*], Guoying Wang[1], Hongmei Chen[1], and XinMing Zhang[2]

[1]School of Materials Science and Engineering, Jiangsu University of Science and Technology, Zhenjiang 212003, China
[2]Key Laboratory of Nonferrous Metal Materials Science and Engineering, Ministry of Education, Central South University, Changsha 410083, China

(received date: 16 May 2017 / accepted date: 24 June 2017)

The effect of grain size inhomogeneity of large ingot on the hot deformation behavior of Al-8Zn-2Mg-2Cu alloy were investigated using hot compression tests over a temperature range from 300 °C to 450 °C with strain rate from 0.1 s^{-1} to 10 s^{-1}. It was found that the grain size (100 μm) in surface layer of the ingot is finer than that of the central layer (>200 μm). The surface specimen exhibited lower flow stress than that of central one in the temperature range from 350 °C to 450 °C and the strain rate range from 0.1 s^{-1} to 1 s^{-1}. The softening mechanism is dynamic recovery, together with a partial dynamic recrystallization (DRX) at high temperature and low strain rate condition regardless the grain size. The nucleation mechanism of DRX is the strain induced grain boundary migration. Therefore, the DRX fraction is higher in surface specimen because the higher grain boundary density provides more nucleation sites. Based on processing maps, the applicable hot deformation parameters for the large size ingot are determined to be at the temperature range of 440-450 °C and the strain rate of 0.1-0.3 s^{-1} when taking the grain size inhomogeneity into account.

Keywords: alloys, hot working, microstructure, dynamic recovery, dynamic recrystallization

1. INTRODUCTION

The thick rolled plate of a high strength Al–8Zn–2Mg–2Cu alloy will be produced as the siding of wing in Chinese big plane project [1]. The industrial process of this high strength aluminum alloy to produce thick plate involves casting, homogenization, hot rolling, solution and ageing. Each processing step has certain influence on the microstructural evolution in subsequent stages [2]. For example, due to the through-thickness inhomogeneity of deformed microstructure in hot rolled thick plate and the major influence on the static recrystallization in solution [3], it is necessary to understand the effect of ingot microstructure inhomogeneity on the structure refinement during deformation. Therefore, the precise prediction of flow stress during rolling process and the analysis of hot deformation behavior for various original microstructures are especially important to the establishment of hot rolling technique and the optimization of final properties.

Parsa and Ohadi [4] investigated the effect of initial grain size on the constitutive equation[5] and recrystallization maps [6] for a stainless steel. The relationship of grain size and deformation mechanism to the fracture behavior in nanostructured austenitic stainless steel was researched by Misra *et al.* [7]. The effects of initial grain size on hot deformation behavior of commercial pure aluminum was also reported [8]. The results indicated that the flow stress decreases with the grain size decreasing under low strain rate condition. Yang *et al.* [9] studied the effects of grain size on the hot deformation behavior and processing map for 7075 alloy. It was concluded that the flow stress of the alloy with coarse grains was higher than that of the alloy with fine grains. Unlike the steel and 7075 aluminum alloy, Chan and Fu *et al.* found that the decrease of flow stress for pure copper was caused by the dwindling of grain boundary strengthening effect when the grain size was increased [10]. The experimental results and conclusions about the effect of grain size on the deformation behavior were various due to the different composition and crystal structure of experimental materials.

Based on the researches about the microstructure of large scale ingot with the composition similar to that of our research, it was known that there was through-thickness grain size inhomogeneity due to the gradient of cooling rate after casting or homogenization [2]. The hot deformation behaviors of the microstructure in different layers may be different due to the various original grain sizes. Therefore, the through-thickness

*Corresponding author: difeng1984@just.edu.cn

inhomogeneity of deformation microstructure or deformation stored energy was brought about [11], resulting in the difference of grain morphology, and the inhomogeneity of dynamic or static recrystallization degree. However, the effects of initial grain size inhomogeneity of large size ingot on the hot deformation behavior or the final grain morphology of high strength aluminum alloy rolled plate had not been reported.

In this paper, the grain size inhomogeneity in large scale ingot of a Al–8Zn–2Mg–2Cu alloy was analyzed firstly. Samples with different grain size were chosen to investigate the varieties of the hot deformation behavior using hot compression test. The dynamic material models (DMM) based processing maps were established for different original microstructure samples. Finally, the optimum hot deformation parameters were determined when taking the grain size inhomogeneity of the large size ingot into account. The purpose of our research was to investigate the relationship between original microstructure inhomogeneity and the grain redefined mechanism during hot deformation, and to establish the applicable rolling technique for the large scale ingot with microstructure through-thickness inhomogeneity.

2. EXPERIMENTAL PROCEDURE

2.1. Sample preparation and deformation

The material used in this study was taken from an industrial ingot provided by the Aluminum Corporation of China Ltd with nominal compositions of Al–8Zn–2Mg–2Cu (in wt%). The ingot was industrially homogenized at 470 °C for 48 h and then air cooling. The sampling positions in current study are depicted by point A and point B in Fig. 1, and the actual chemical compositions of the two positions were measured by Direct-reading Spectrometer. Cylindrical specimens of 10 mm in diameter and 15 mm in height were machined for hot compression tests from the surface layer (position A) and central layer (position B), respectively, as shown in Fig. 2(a). Hot compression tests were carried out on a Gleeble-3500 simulator at temperatures from 300 °C to 450 °C with strain rates

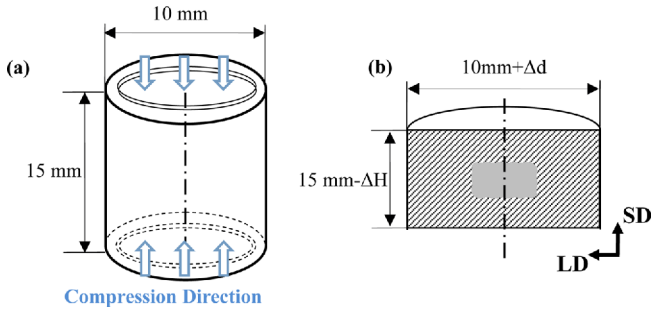

Fig. 2. Schematic of sample before and after compression; (a) The sample before compression (Arrows represent compression direction) and (b) Half of the compressed sample sectioned parallel to the compression axis along the direction of centerline (The box filled with grey represents the position of TEM and EBSD observation. ΔH is the compressed reduction. Δd is the increasment of diameter).

from 0.1 s^{-1} to 10 s^{-1}. Before compression, the samples were heated to the deformation temperatures at a rate of 2 °C/s, and then held for 3 min to homogenize the temperature of the sample. All specimens were compressed to about 65% reduction, which corresponds to a true strain of approximately 1, and then quenched in water quickly after each compression to freeze the deformation microstructures.

The deformed samples were sectioned parallel to the compression axis along the direction of centerline. All microstructure observations were examined at the central positions on the SD-LD plane of the samples, as depicted in Fig. 2(b). The grains and dislocations were observed by the TecnaiG^2 20 transmission electron microscope (TEM) and Sirion 200 field emission gun scanning electron microscope (SEM) equipped with EBSD system. The TEM and EBSD samples were the thin foils with thickness of 80 μm and diameter of 3 mm, which were electropolished in a solution containing 20%HNO_3 in methanol at ~ -25 °C and 15-20 V. On account of detection limitation in hot worked structure [1,12], boundaries with a misorientation angle of less than 2° were not taken into account for EBSD observation. The step size between points on the scan grid was set to 2.5 μm.

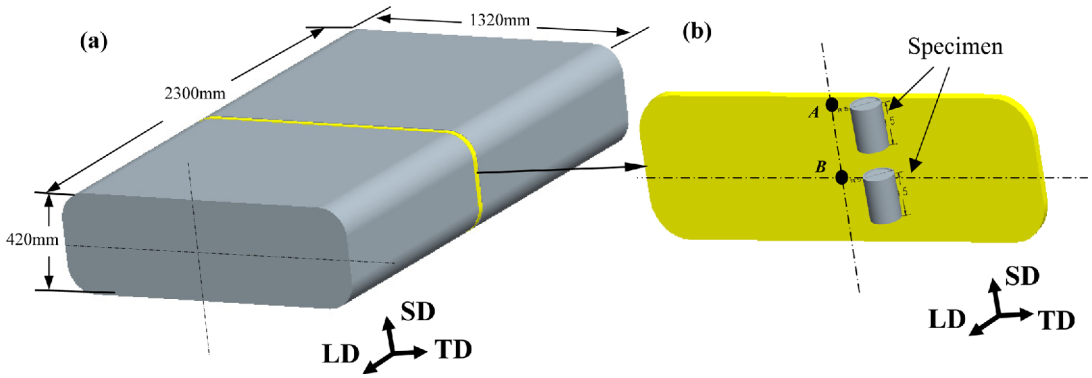

Fig. 1. The schematic diagram of sampling; (a) The scale of the ingot and (b) Sampling positions (A and B represent the sampling positions in surface layer and central layer, respectively).

2.2. Approach of processing map

The basis for the processing map is the dynamic materials model [13-18]. Research revealed that the total power P from hot deformation could be described as follow:

$$P = G + J = \sigma\dot{\varepsilon} = \int_0^{\dot{\varepsilon}} \sigma d\dot{\varepsilon} + \int_0^{\sigma} \dot{\varepsilon} d\sigma \quad (1)$$

where G content and J co-content are two complementary parameters. G represents the power dissipation through plastic deformation. J represents power dissipation through microstructural evolution.

The efficiency of power dissipation is given as:

$$\eta = \frac{2m}{1+m} \quad (2)$$

where m is the strain rate sensitivity. High η value indicates that power dissipation could supply more energy for DRX or DRV.

The extremum principles of irreversible thermodynamics as applied to continuum mechanics of large plastic flow are explored to define a criterion for the onset of flow instability given by the equation for the instability parameter ξ:

$$\xi = \frac{\partial \lg[m/(m+1)]}{\partial \lg \dot{\varepsilon}} \quad (3)$$

The three-dimensional variation of the efficiency of power and dissipation instability parameter as a function of temperature and strain rate represents a processing map. Processing map reveals the deterministic domains where individual microstructural processes occur and the limiting conditions for the regimes of flow instability. By processing under conditions of the highest efficiency in the "safe" domains and by avoiding the regimes of flow instabilities, the intrinsic workability of the material may be optimized and microstructural control may be achieved.

3. RESULTS AND DISCUSSION

3.1. The inhomogeneity analysis of ingot

Figure 3 shows the microstructure of both surface and central layer specimens of the ingot. The micrograph consists of approximate equiaxed grains with diameter of about 100 μm for surface layer specimen (Fig. 3(a)). For central layer specimen, the grain size is larger than 200 μm (Fig. 3(b)). Coarse precipitates in the grain boundary (GBPs) and relative fine particles in the matrix are observed. The bulk of aluminum alloy billet after industrial homogenization are all cooled in air at room temperature, and the cooling time may be 20h or more for large ingot. Therefore, a large number of second phase particles precipitated and even coarsened during this course. However, the morphologies or densities of the precipitates and coarsened phases are almost the same. The chemical compositions of the surface layer specimen (position A) and the center one(position B) of the homogenized ingot are shown in Table 1. Although the composition segregation results in a difference in the content of main alloying elements, the chemical composition inhomogeneity is invisible. The content of Zn, Mg and Cu at the surface layer are only 1.01, 1.02 and 1.02 times of that at the center, and the Zn:Mg ratios are almost the same for both layers. In other words, these reasonable variations of chemical composition is permitted.

Therefore, the chemical composition inhomogeneity of the large ingot in our study was considered has no influence on the deformation behavior of the alloy when compared to the grain size inhomogeniety between surface and central layer. In current paper, the specimen with fine grain is defined as

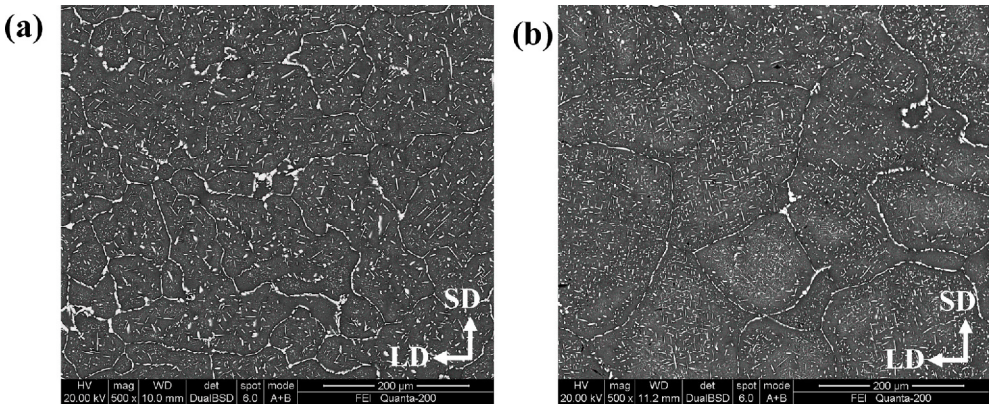

Fig. 3. The inhomogeniety of ingot microstructures; (a) surface of ingot and (b) center of ingot.

Table 1. Chemical compositions at the surface and center of the received ingot (wt%)

Position	Zn	Mg	Cu	Zr	Fe+Si	Al
Surface	8.01	2.14	2.11	0.13	0.1	Bal
Center	7.93	2.09	2.07	0.14	0.1	Bal

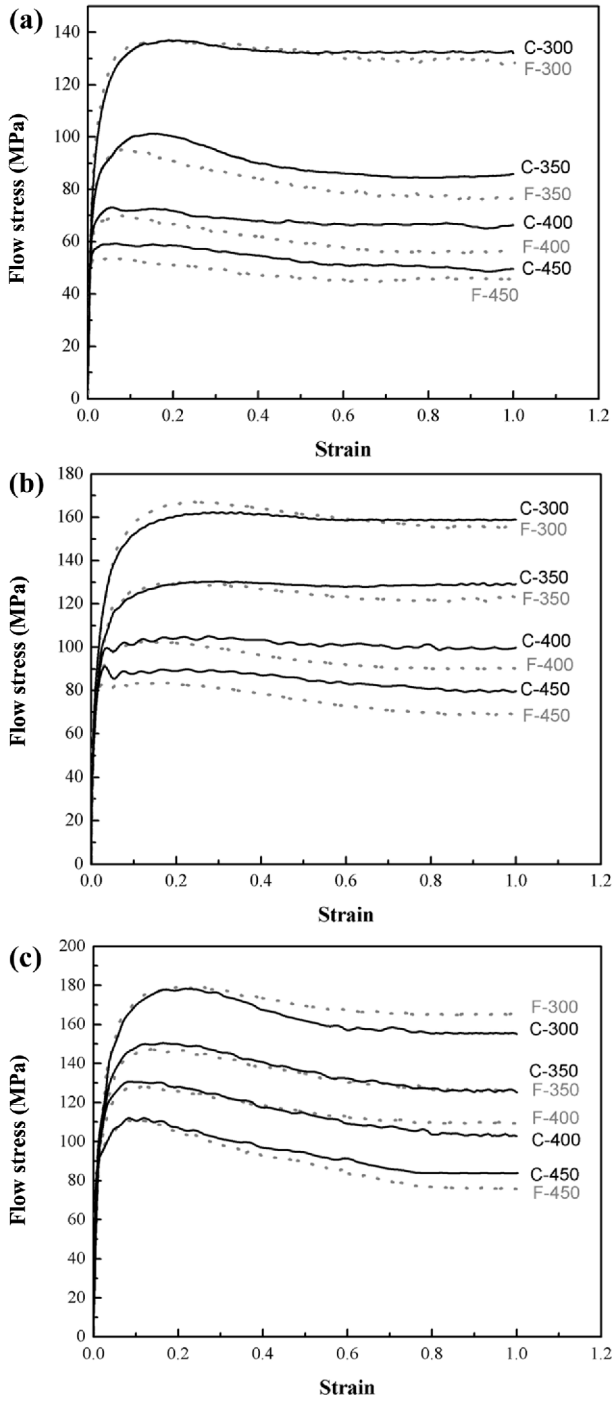

Fig. 4. Typical flow curves for different temperatures, strain rates, and initial grain sizes (F/C-temperature represents the fine/coarsen specimen deformed under different temperature); (a) 0.1 s^{-1}, (b) 1 s^{-1}, and (c) 10 s^{-1}.

F-specimen (surface layer specimen), and the specimen with coarse grain was defined as C-specimen (central layer specimen).

3.2. Flow stress

The flow stress curves of F-specimen and C-specimen under various deformation conditions are shown in Fig. 4. The results show that, whatever the initial grain size is, the flow stress increases quickly with the increase of true strain at the initial deformation stage, and then keeps steady or decreases to a certain extent lower than the peak stress. It is also show that, the flow stress declines with an increase of deformation temperature and a decrease of strain rate. However, some different phenomena can be summarized below.

(1) Under the high temperature and low strain rate conditions, the flow stress of F-specimen is lower than that of C-specimen at the same strain value. For example, at the temperature of 450 °C and the strain rate of 0.1 s^{-1} (Fig. 4(a)), the flow stress is about 53 MPa for C-specimen but 45 MPa for F-specimen when the true strain value is 0.7. When the strain rate is 1 s^{-1} and the temperature is 450 °C, the flow stress has reached to 85 MPa for C-specimen but 70 MPa for F-specimen (Fig. 4(b)).

However, the difference between the two stress levels decreases with strain rate increasing and temperature decreasing. For example, at the temperature of 300 °C, the two flow stress values are almost the same, as depicted in Fig. 4.

(2) The range of flow stress becomes tighter with increasing initial grain size. For example, when the strain rate is low (0.1 s^{-1} or 1 s^{-1}), the stress differences between different temperatures at the same strain rate are higher in F-specimen than that of C-specimen. This is due to the low stress extent of F-specimen under high temperature and low strain rate condition.

In fact, there is a competition between work hardening and dynamic softening during hot deformation. The potential driving forces of dynamic softening behavior (DRX or DRV) increase with the increasing of the strain and temperature. DRX or DRV reorganizes the dislocation structure and reduces its density. When the dynamic softening and work hardening reach a dynamic equilibrium, the flow stress reduces to a steady value. Thus, the enhancement of certain dynamic softening behavior in F-specimen contributes to the low flow stress compared with C-specimen under high temperature and low strain rate condition.

3.3. The mechanism of dynamic softening

3.3.1. The mechanism of DRV

TEM microstructures under different deformation conditions for both specimens are shown in Fig. 5. Under the higher strain rate and lower temperature (350 °C and 10 s^{-1}), the sub-grains are elongated with thick walls of very tangled dislocations (Figs. 5(a,d)), and the sub-grains are relatively small. As the temperature increasing and strain rate decreasing (450 °C and 1 s^{-1}), the dislocations collect into more widely spaced and less dense tangles. The sub-grains increase in diameter with more clearly defined sub-grain boundaries containing dislocations in an orderly fashion, as shown in Figs. 5(b,e). As the strain rate decreases to 0.1 s^{-1} with the deformation temperature of 450 °C (Figs. 5(c,f)), the larger sub-grains with straight

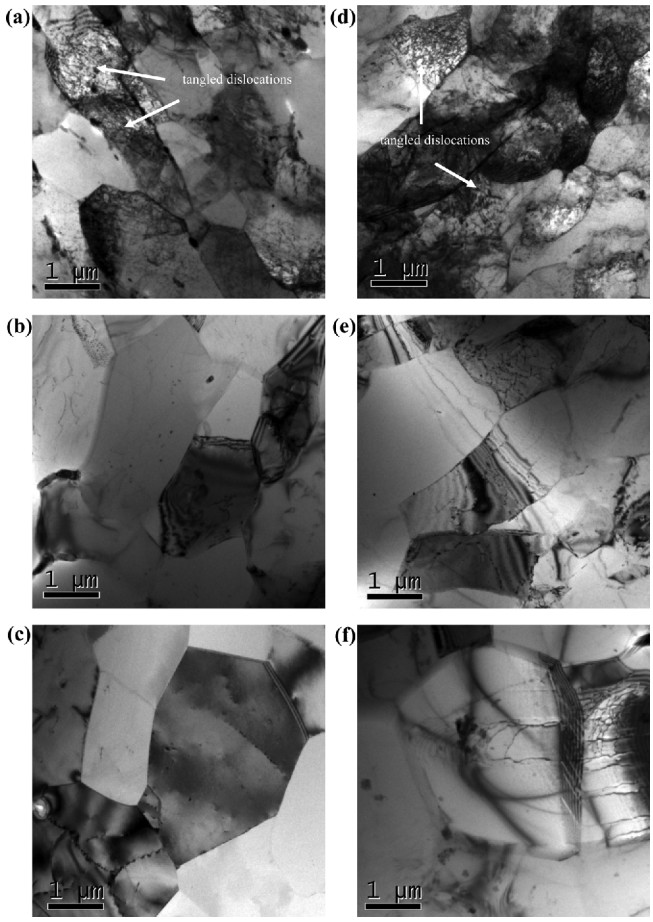

Fig. 5. TEM microstructures deformed under different conditions. F-specimen: (a) 350 °C and 10 s^{-1}, (b) 450 °C and 1 s^{-1}, (c) 450 °C and 0.1 s^{-1}; C-specimen: (d) 350 °C and 10 s^{-1}, (e) 450 °C and 1 s^{-1}, (f) 450 °C and 0.1 s^{-1}.

grain boundaries and lower dislocation density are found. It can be concluded that, with the increasing of temperature and the decreasing of strain rate, the dislocation tangles reorganized into subgrains with walls that are more widely spaced and straighter, and includes fewer, more regularly arranged dislocations [12]. There is no doubt that the main softening mechanism of Al–8Zn–2Mg–2Cu alloy is dynamic recovery in our study.

For the purpose to investigate the dynamic recovery mechanism for both of the two specimens, the thermal activation parameters are analyzed. The activation energy (Q) is a characterization serving as an indicator of atomic rearrangement difficulty. Otherwise, the calculation of Q is not based on any theoretical model or atomistic rate-controlling mechanism. A more rigorous equation has been found very useful, and an important conception called activation volume is defined as follows:

$$V = kT\left[\frac{\partial \ln \dot{\varepsilon}}{\partial \sigma}\right] \quad (4)$$

Table 2. Activation volume V (b is Burger's vector)

T (°C)	V (b^3)		
	0.1 s^{-1}	1 s^{-1}	10 s^{-1}
	F-specimen		
300	30	25.5	20.5
350	29.3	25.4	21
400	33.2	26.6	20
450	34.1	34.1	34.1
	C-specimen		
300	24.3	23.1	22
350	30.7	24.6	17
400	37.5	32.4	26.1
450	38.5	36.7	35

where V is the activation volume, k is Boltzman constant and T is the absolute temperature. The activation volumes are shown in Table 2 for different grain size specimens, respectively.

Dynamic recovery mechanism includes the dislocation slip or cross slip, dislocation climb, non-conservative motion of jogs and unzipping of attractive junctions. Different mechanism corresponds to a certain activation volume value [19]. The estimated V values in the range of (15-40b^3) increase with increasing temperature no matter what the grain size is. The activation volume ranges suggest that the mechanism of dynamic recovery is cross-slip.

3.3.2. The mechanism of DRX

In an attempt to gain more insight into microstructural evolution during the hot deformation, IPF maps are generated under typical deformation conditions, as shown in Figs. 6 and 7.

Figure 6 shows the typical microstructures and corresponding misorientation angle distribution maps of F-samples under various deformation conditions. From Figs. 6(a,c,e), it can be seen that, the grains are pressed flat after deformation. The microstructure consists of deformed grains characterized by high angle boundary (HAB). Additionally, the original grain boundaries become serrated (serrated GB, as marked in Figs. 6(a,c,e)). This morphology is related to the migration of high grain boundaries in response to both the boundary tensions of the substructure and to variations in dislocations, which indicates a stronger DRV behavior. As the temperature increasing or strain rate decreasing, fine and equiaxed grains are obviously observed, which can be seen in the areas surrounded by the box of black dot line in Figs. 6(c,e). As we all known that dynamic recrystallization takes place when a critical deformation condition is reached. Generally, new grains originate at the initial grain boundaries, but, as the specimens continue to deform, the dislocation density of the new grains increases, thus reducing the driving force for further growth, and the recrystallizing grains eventually cease to grow. Therefore, the fine and equiaxed grains are always observed on the grain

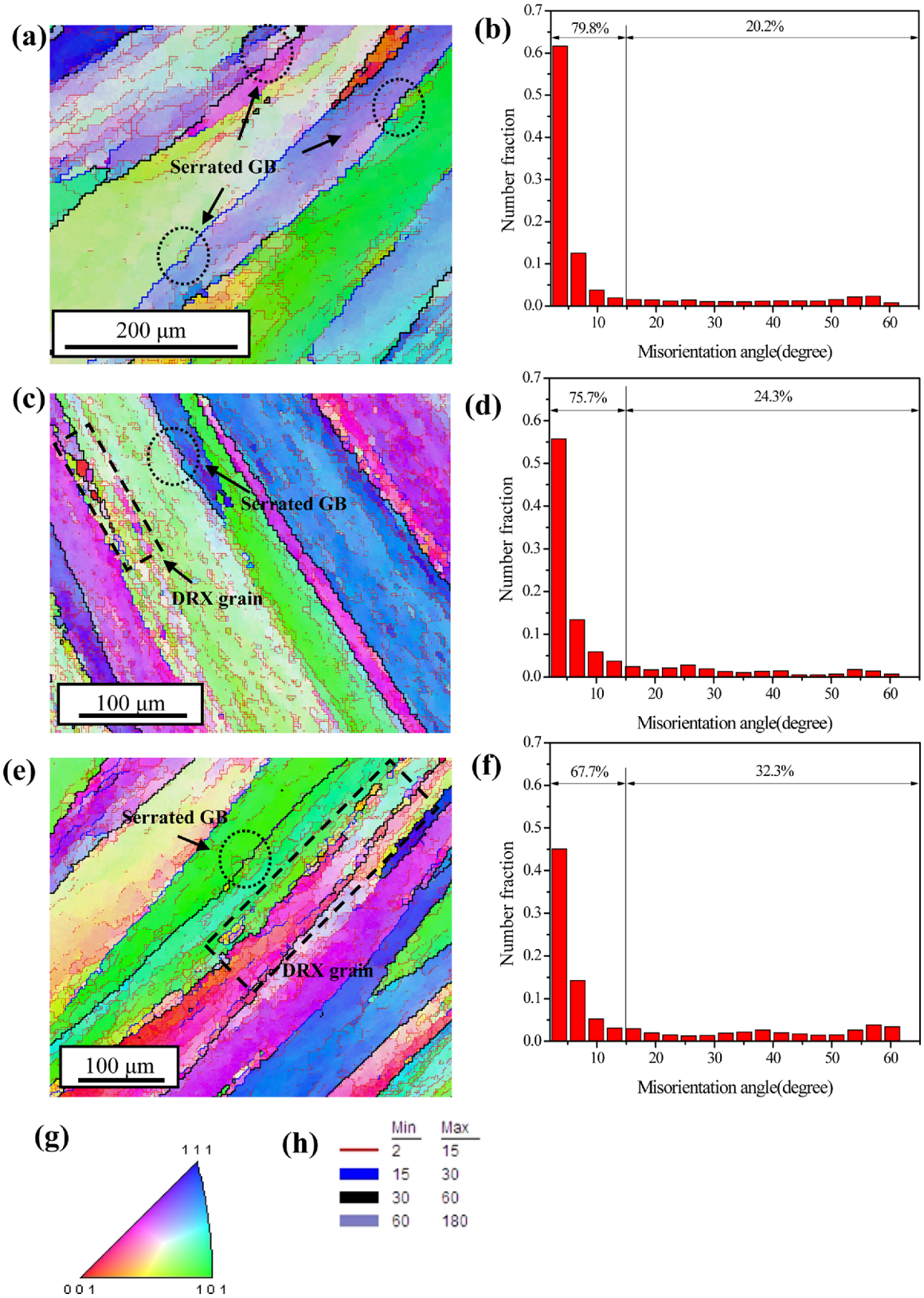

Fig. 6. IPF maps and misorientation angle distribution of F-specimen conducted at different deformation conditions (ε=1); (a,b) 450 °C-1 s^{-1}, (c,d) 400 °C-0.1 s^{-1}, (e,f) 450 °C-0.1 s^{-1}, (g) representation of the color code used to identify the crystallographic orientations on standard stereographic projection (red: [001]; blue: [111]; green: [101]), and (h) representation of different color lines used to identify the boundaries with different misorientation angles.

boundaries.

Figures 6(b-f) give the statistical results of grain boundary misorientation under different deformation conditions. With the decrease of strain rate or the increase of compressed temperature, a continuous decrease from 79.8% to 67.7% in low angle boundaries (below 15°) and a steady increase from 20.2% to 32.8% in the high angle boundaries (above 15°) were observed. Such an evolution can be referred to as continuous dynamic recrystallization, according to the researches of Gourdet and Montheillet [20]. In our study, small equiaxed grains were obviously observed in OIM (shown in Figs. 6(c,e)). Thus dynamic recrystallization had occurred at high temperature and low strain rate condition, which confirmed the analysis of stress-strain curve and TEM observations.

Figures 7(a,c) show the typical microstructures of C-specimen under various deformation conditions. Similar to the character of F-specimen, flat grains are also observed and the microstructure mostly consisted of deformed grains is characterized by high angle boundary (HAB). Serrated grain boundaries are presented (Figs. 7(a,c)). However, there are only few

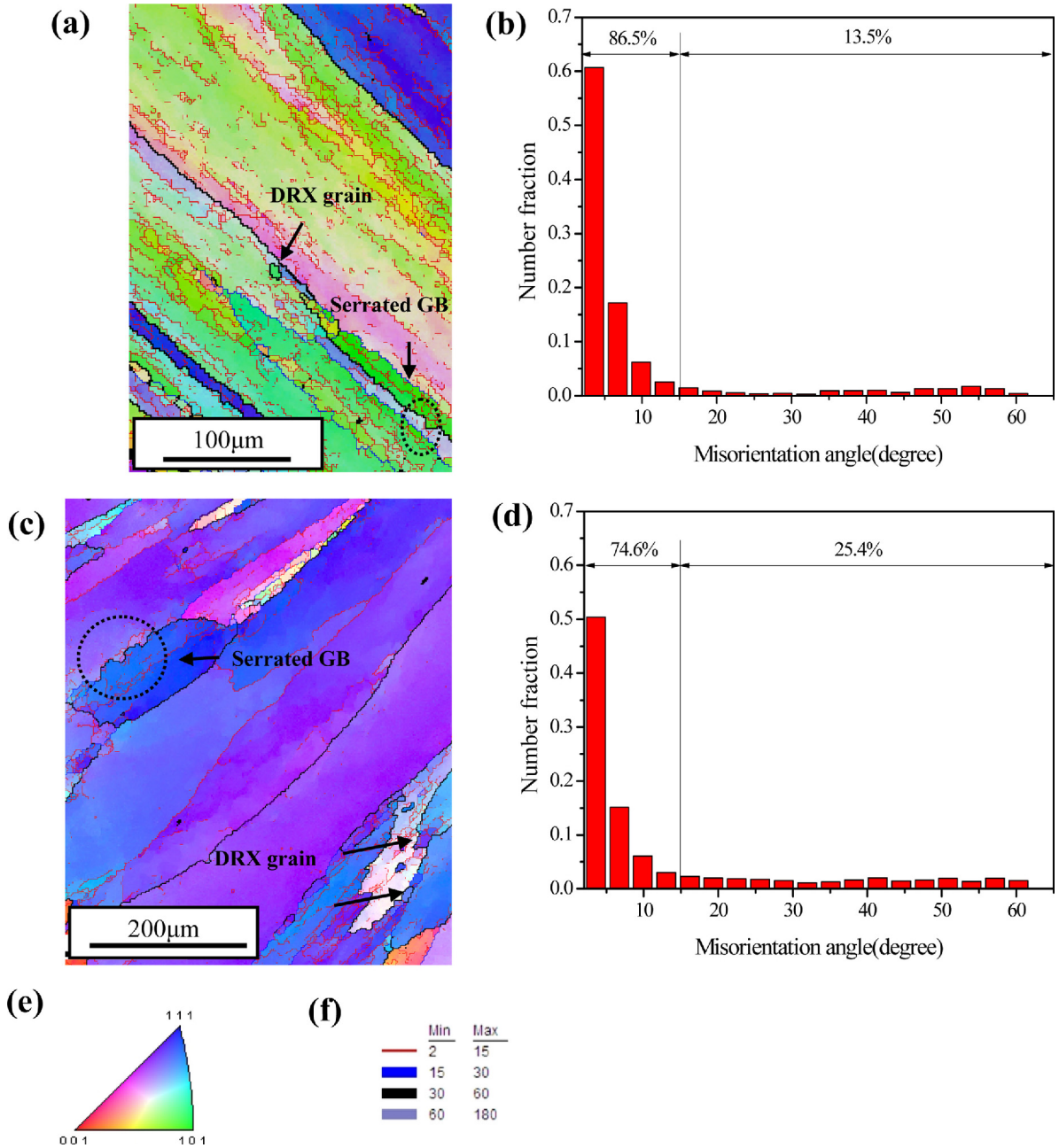

Fig. 7. Microstructures of C-specimen conducted at different deformation conditions (ε=1); (a,b) 450 °C-1 s^{-1}, (c,d) 450 °C-0.1 s^{-1}, (e) representation of the color code used to identify the crystallographic orientations on standard stereographic projection (red: [001]; blue: [111]; green: [101]), and (f) representation of different color lines used to identify the boundaries with different misorientation angles.

equiaxed DRX grains (Fig. 7(c)) at the same hot compression conditions compared with F-specimen in our study. It means that the DRV is also the dominated dynamic softening behavior and the DRX fraction is evidently lower than that of F-specimen. The statistical results of grain boundary in Fig. 7(b,e) shows a similar evolution law to that of F-specimen. In other words, the increase of the higher angle boundaries (above 15°) and the decrease of low angle boundaries (above 15°) are also observed. That is to say, the continuous DRX also occurred in C-specimen under high temperature and low strain rate conditions. However, the number fraction of high angle boundaries (above 15°) under the same compressed condition is higher in F-specimen when compared Figs. 7(b,d) to Figs. 6(b,f). Results show that, the DRX fraction is higher in F-specimen than that of C-specimen when hot deformed under the same conditions.

Due to the low driving force and large interfacial energy, the classical nucleation of dynamic recrystallization can be discounted, while strain induced grain boundary migration (SIBM) is convictive. SIBM involves the bulging of part of a pre-existing grain boundary, leaving a region behind the migrating boundary with lower dislocation content. As a result, this area without strain will become a dynamic recrystallization nucleus when critical size is reached [21]. In our study, the alloy exhibits an evident dynamic softening behavior in high temperature and low strain rate. The EBSD map of SIBM for C-specimen deformed at 400 °C-0.1 s^{-1} is shown in Fig. 8. Several serrated boundaries migrate to the direction marked by arrows in Fig. 8. However, the stored energy difference between the two original grains is proofless. Research [21] revealed that, if SIBM in a material with well recovered sub-grains, it may originate at a single large sub-grain. For single sub-grain SIBM there is no requirement for a stored energy difference in the two neighboring grains, merely that there is a sub-grain of the critical size adjacent to the grain boundary. As depicted in Fig. 8, the recrystallized grain and the sub-grain adjacent to the serrated boundaries is about 8 μm, which can be considered as the critical size for DRX in our study.

It can be concluded that, DRV behavior exists in a wider deformation condition range while DRX only occurs at high temperature and low strain rate conditions for both specimens, which means that the softening mechanism of the aluminum alloy in our study is DRV, together with a partial DRX at high temperature and low strain rate conditions no matter what the grain size is. However, the nucleation mechanism of DRX is single sub-grain strain induced grain boundary migration (SIBM). Therefore, the DRX fraction is higher in surface specimen (F-specimen) because the higher grain boundary density provides more nucleation sites.

3.4. Processing map

The DMM based processing maps obtained at the strain of 1.0 for both F-specimen and C-specimen are shown in Fig. 9.

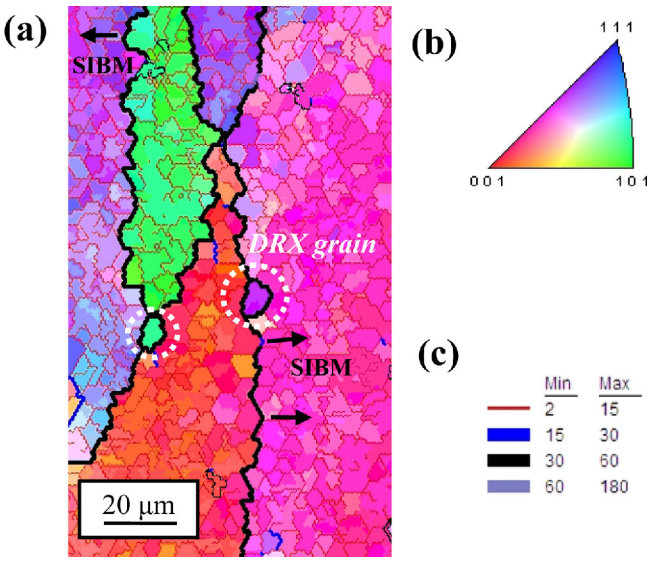

Fig. 8. EBSD observation; (a) SIBM in C-specimen (400 °C-0.1 s^{-1}, black arrows represent the direction of SIBM), (b) representation of the color code used to identify the crystallographic orientations on standard stereographic projection (red: [001]; blue: [111]; green: [101]), and (c) representation of different color lines used to identify the boundaries with different misorientation angles.

The details of graphic method can be seen in Refs.[13-18,22]. The color against each domain between contours represents the efficiency of power dissipation as percent. The domains in the two maps below the red dot line are the safety regimes while the ones above the line represent the regime of flow instability. The instability domains of both types of specimens locate at the relative high strain rate range.

There are two safety domains in the processing map regardless the initial grain size. However, the corresponding temperature range and strain range are different. For F-specimen (Fig. 9(a)), the first safety domain is below the instability area and lies in the area with the strain rate above 0.1 s^{-1} (I in Fig. 9(a)). The second one locates at the slow strain rate (<0.1 s^{-1}) range under the whole temperature condition in our study (II in Fig. 9(a)). For C-specimen, the first safety domain is also below the instability one but lies in the area with the strain rate above 1 s^{-1} (I in Fig. 9(b)). The second one locates at the slow strain rate (1 s^{-1}) range under the whole temperature condition (II in Fig. 9(b)). That is to say, the C-specimen has a larger safety deformation conditions range. Besides, the peak efficiency value is 48.3% for F-specimen while 38.9% for C-specimen. The difference of peak efficiency value means that more microstructure evolution occur during deformation of F-specimen than that of C-specimen. In high metallic materials, the maximum efficiency of power dissipation for DRX is 35% of high stacking fault material [23]. Therefore, the dynamic softening behavior in the peak efficiency area results from DRX for both types of specimens while the DRX extent is more evident in F-specimen. The analysis of efficiency of power dis-

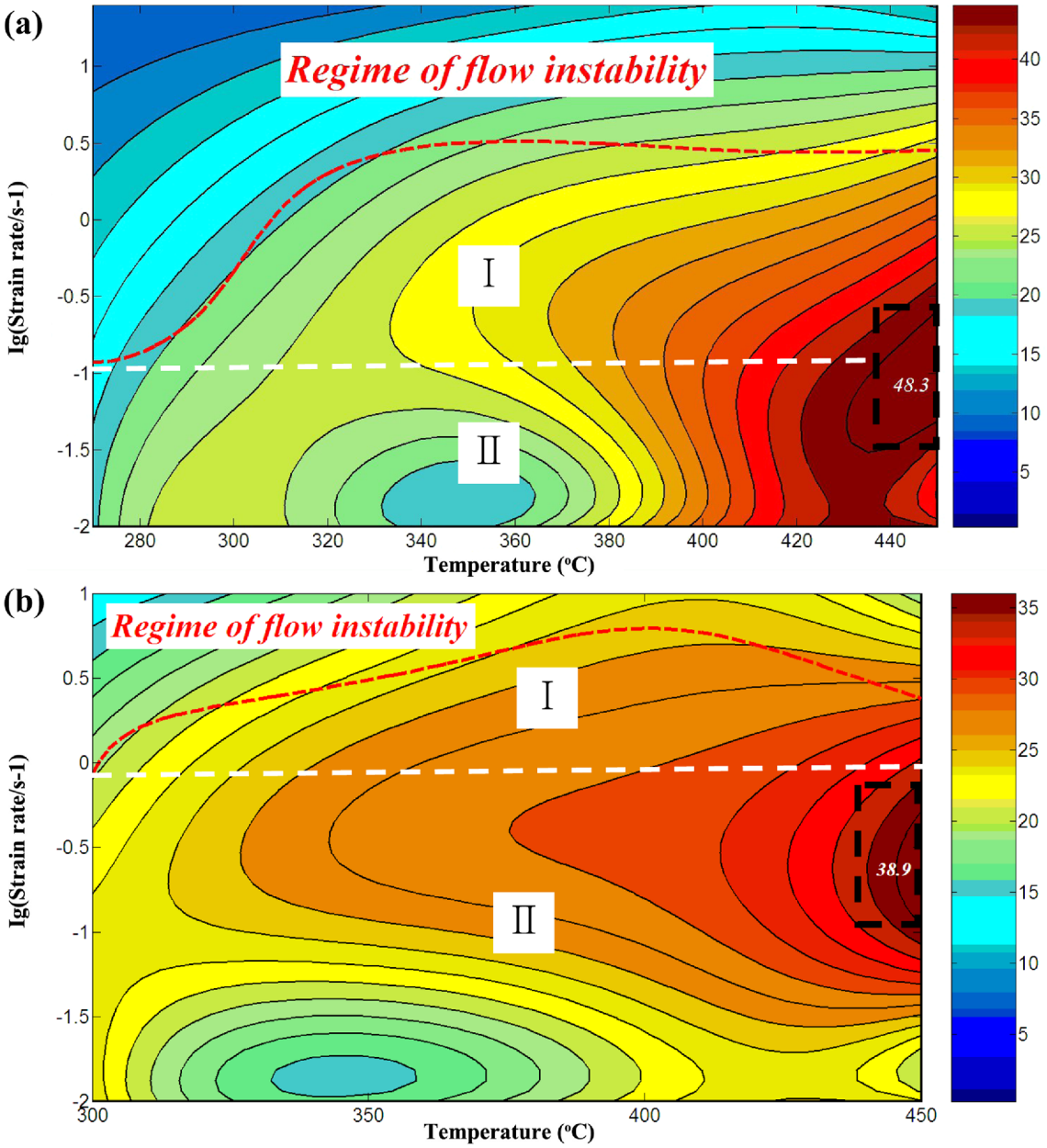

Fig. 9. Processing maps for homogenized Al–8Zn–2Mg–2Cu alloy at the true strain of 1; (a) Processing map of F-specimen and (b) Processing map of C-specimen.

sipation based on processing map coincides with that of TEM and EBSD observations.

Based on processing map and microstructure observations, the optimum hot deformation parameters are determined to be at the temperature range of 440-450 °C and strain rate range of 0.1-0.5 s^{-1} for coarse grain microstructure, while at the temperature range of 420-450 °C and the strain rate below 0.3 s^{-1} for fine grain microstructure. Therefore, the applicable hot deformation parameters for the hot rolling processing of large ingot are determined to be at the temperature range of 440-450 °C and the strain rate of 0.1-0.3 s^{-1} when taking the grain size inhomogeneity of ingot into account.

4. CONCLUSION

In this paper, the grain size inhomogeneity in large scale ingot of Al–8Zn–2Mg–2Cu alloy was analyzed. Specimens with different grain size were chosen to investigate the varieties of the dynamic softening behavior. The optimum hot deformation parameters were determined when taking the grain size inhomogeneity of the large size ingot into account. The main results can be summarized as follows:

(1) The grain size in surface layer of the ingot is about 100 μm, which is finer than that of the central layer (>200 μm). The flow stress of the specimen with fine grain is lower than

that of the specimen with coarse grain at 350-450 °C and 0.1-1 s^{-1} range.

(2) The softening mechanism of the Al-Zn-Mg-Cu alloy in our study is dynamic recovery (DRV), together with a partial DRX at high temperature and low strain rate condition regardless the grain size. However, the nucleation mechanism of DRX is the single sub-grain strain induced grain boundary migration (SIBM). Therefore, the DRX fraction is higher in fine grain microstructure because the higher grain boundary density provides more nucleation sites.

(3) Processing maps at the strain of 1 are established for both of the two specimens. The optimum hot deformation parameters are determined to be at the temperature range of 440-450 °C and strain rate range of 0.1-0.5 s^{-1} for coarse grain microstructure, while at the temperature range of 420-450 °C and the strain rate below 0.3 s^{-1} for fine grain microstructure. The applicable hot deformation technique for the hot rolling of large ingot can be collected to locate at the temperature range of 440-450 °C and the strain rate of 0.1-0.3 s^{-1} when taking the grain size inhomogeneity of ingot into account.

ACKNOWLEDGEMENT

This work was financially supported by the National Basic Research Program (973) of China (No.2012CB619505), National Natural Science Foundation of China (No.51301077), Natural Science Fund project in Jiangsu Province (No.BK20160560) and the Natural science fund for colleges and universities in Jiangsu Province (No.16KJB430010).

REFERENCES

1. D. Feng, X. M. Zhang, S. D. Liu, and Y. L. Deng, *Mat. Sci. Eng. A* **608**, 63 (2014).
2. J. D. Robson, *Mat. Sci. Eng. A* **382**, 112(2004).
3. Z. B. Li, J. Shen, L. M. Yan, J. P. Li, X. D. Yan, and B. Q. Mao, *Chin. J. Rare Met.* **34**, 643 (2010).
4. M. H. Parsa and D. Ohadi, *Mater. Design* **52**, 412 (2013).
5. H. Mirzadeh, M. H. Parsa, and D. Ohadi, *Mat. Sci. Eng. A* **569**, 54(2013).
6. D. Ohadi, M. H. Parsa, and H. Mirzadeh, *Mat. Sci. Eng. A* **565**, 90 (2013).
7. R. D. K. Misra, X. L. Wan, V. S. A. Challa, M. C. Somani, and L. E. Murr, *Mat. Sci. Eng. A* **626**, 41 (2015).
8. H. R. Rezaei Ashtiani, M. H. Parsa, and H. Bisadi, *Mater. Design* **52**, 478 (2012).
9. Y. B. Yang, Z. M. Zhang, X. B. Li, Q. Wang, and Y. H. Zhang, *Mater. Design* **51**, 592 (2013).
10. W. L. Chan, M. W. Fu, J. Lu, and J. G. Liu, *Mat. Sci. Eng. A* **527**, 6638 (2010).
11. L. Zhen, J. Z. Chen, S. J. Yang ,W. Z. Shao, and S. L. Dai, *Mat. Sci. Eng. A* **504**, 55 (2009).
12. Y. Deng, Z. M. Yin, and J. W. Huang, *Mat. Sci. Eng. A* **528**, 1780 (2011).
13. K. P. Rao, Y. V. R. K. Prasad, and K. Suresh, *Mater. Design* **32**, 2545 (2011).
14. K. P. Rao, Y. V. R. K. Prasad, C. Dharmendra, N. Hort, and K. U. Kainer, *Mat. Sci. Eng. A* **528**, 6964 (2011).
15. Y. V. R. K. Prasad, K. P. Rao, N. Hort, and K. U. Kainer, *Mat. Sci. Eng. A* **502**, 25 (2009).
16. Y. V. R. K. Prasad, K. P. Rao, N. Hort, and K. U. Kainer, *Mater. Lett.* **26**, 4207 (2008).
17. N. Srinivasan, Y. V. R. K. Prasad, and K. P. Rao, *Mat. Sci. Eng. A* **476**, 146 (2008).
18. Y. V. R. K. Prasad and K. P. Rao, *Mat. Sci. Eng. A* **374**, 335 (2004).
19. K. P. Rao and Y. V. R. K. Prasad, *J.Mech. Sci. Technol.* **13**, 86(1986).
20. S. Gourdet and F. Montheillet, *Acta Mater.* **51**, 2685(2003).
21. F. J. Humphreys and M. Hatherty, *Recrystallization and Related Annealing Phenomena, 2nd ed.*, pp.251-253, Elsevier, Oxford, UK (2004).
22. D. Xiao, X. Y. Peng, X. P. Liang, Y. Deng, G. F. Xu, and Z. M. Yin, *Met. Mater. Int.* **23**, 591 (2017).
23. G. Meng, B. L. Li, H. M. Li, H. Huang, and Z. R. Nie, *Mat. Sci. Eng. A* **517**, 132 (2009).